

Long-lived Sterile Neutrino Searches at Future Muon Colliders

Qi Bi,^{1,a} Jinhui Guo,^{1,b} Jia Liu,^{2,3,c} Yan Luo,^{2,d} and Xiao-Ping Wang^{1,4,e}

¹*School of Physics, Beihang University, Beijing 100083, China*

²*School of Physics and State Key Laboratory of Nuclear Physics and Technology, Peking University, Beijing 100871, China*

³*Center for High Energy Physics, Peking University, Beijing 100871, China*

⁴*Beijing Key Laboratory of Advanced Nuclear Materials and Physics, Beihang University, Beijing 100191, China*

Abstract

We explore the potential of studying sterile neutrinos at a future high-energy muon collider, where these particles can generate small active neutrino masses via the seesaw mechanism and exhibit long-lived particle signatures. A Dirac sterile neutrino model with $U(1)_{L_\mu-L_\tau}$ symmetry is introduced, where the heavy right-handed neutrino (N_R) produces tiny active neutrino masses, and the light left-handed neutrino (N_L) naturally behaves as a long-lived particle. The $U(1)_{L_\mu-L_\tau}$ gauge symmetry also enhances sterile neutrino pair production at a future high-energy muon collider. Using the displaced vertex method, the muon collider can search for heavy sterile neutrino, especially for $m_L > m_W$. We find that a muon collider with $\sqrt{s} = 3$ (10) TeV and luminosity $\mathcal{L} = 1$ (10) ab^{-1} can probe N_L masses of $m_L \in [100, 1500$ (5000)] GeV and mixing angles $\theta_{\nu L} \in [10^{-13}, 10^{-6}]$.

^a biqii@buaa.edu.cn

^b guojh23@buaa.edu.cn

^c jiali@pku.edu.cn

^d ly23@stu.pku.edu.cn

^e hcwangxiaoping@buaa.edu.cn

CONTENTS

I. Introduction	3
II. The Model	4
III. Constraints	10
IV. Production at Future Muon Collider	13
V. Long-lived Sterile Neutrino Signals at Muon Collider	16
VI. Conclusions	21
VII. Acknowledgments	22
References	22

I. INTRODUCTION

Neutrino oscillation experiments have shown that at least two generations of neutrinos have small but nonzero masses [1–4], contradicting the Standard Model (SM), which assumes neutrinos are massless. This discrepancy, known as the neutrino mass puzzle, provides a key opportunity to investigate physics beyond the Standard Model (BSM). A natural solution to this puzzle is offered by the seesaw mechanism, which predicts the existence of a heavy right-handed neutrino that mixes with Standard Model neutrinos, giving rise to their tiny masses [5–8]. Numerous experiments have diligently searched for sterile neutrinos, spanning both oscillation experiments and collider studies [9–17].

There are plenty of seesaw models [18–26], which can generate the tiny neutrino mass via a heavy right-handed neutrino. In the type-I seesaw mechanism, if the Dirac mass from the Higgs mechanism is at the MeV scale, the typical sterile neutrino mass is around $m_{\nu_s} \sim 100$ TeV. The corresponding mixing angle between active and sterile neutrinos is constrained by the upper limits on the neutrino mass to approximately $\theta \sim \sqrt{m_\nu/m_{\nu_s}} \sim 10^{-8}$ [27, 28]. However, the heavy mass and extremely small couplings in the canonical type-I seesaw framework make detecting sterile neutrinos challenging. Besides, in other mechanisms, such as linear and inverse seesaw mechanisms [20, 21, 25], the sterile neutrinos can be light with mixing parameters larger than the values required by the type-I seesaw mechanism, while still explaining the tiny active-neutrino masses. As a result, researchers often treat sterile neutrino properties as free parameters when exploring collider phenomenology.

Due to the large QCD backgrounds and the small mixing, searching for sterile neutrinos at LHC and HL-LHC with long-lived signatures helps to increase the sensitivity [29–36]. There have been several studies on searching for long-lived sterile neutrinos that are lighter than gauge bosons at LHC [32, 35, 37–41], where their decays are mainly to three-body final states at this mass range. Moreover, the future high-energy muon collider presents a significant opportunity to explore high-energy scale physics at the TeV level due to its high energy, high luminosity, and reduced background [42–56]. Many studies have investigated the muon collider potential to probe various aspects of both the precision measurements of the SM and BSM [57–64]. The muon collider also opens new avenues for muon-specific research with this novel facility. There have been works searching for promptly decaying sterile neutrinos at the muon colliders in recent years [65–75], while their long-lived signatures are still absent.

Addressing both the neutrino mass and long-lived sterile neutrino signatures at a muon collider is challenging. A promising solution involves introducing sterile neutrinos charged under the $U(1)_{L_\mu-L_\tau}$ model [75–79], which also helps resolve the muon $g - 2$ anomaly. Recent studies [75] have examined the behavior of heavy neutral leptons (HNLs) in this framework, but focusing on the prompt decays of right-handed HNLs. Additionally, research on the $U(1)_{L_\mu-L_\tau}$ gauge boson Z' has primarily investigated processes like $\mu^- \mu^+ \rightarrow \gamma Z'$ with $Z' \rightarrow \mu^- \mu^+$ (or $\tau^- \tau^+$), and $\mu^- \mu^+ \rightarrow \mu^+ \mu^-$ (or $\tau^+ \tau^-$) mediated by Z' [80, 81], focusing on invariant mass reconstruction or modifications to the SM processes to constrain the $U(1)_{L_\mu-L_\tau}$ gauge coupling $g_{Z'}$.

In contrast to previous studies, we investigate a UV-complete model featuring a Dirac sterile neutrino charged under $U(1)_{L_\mu-L_\tau}$, which subsequently splits into two HNLs: a heavy N_R with a mass in the hundreds of TeV range, and a lighter N_L with a mass greater than 100 GeV. The right-handed N_R generates the small mass of SM neutrinos, similar to the type-I seesaw mechanism, while the left-handed N_L is naturally long-lived due to the double suppression from the small neutrino mass and the small Dirac mass of sterile neutrinos. We explore the potential of detecting long-lived N_L at a future high-energy muon collider with $\sqrt{s} = 3$ TeV and 10 TeV, focusing on its pair production through Drell-Yan processes mediated by the new Z' gauge boson. We then explore its subsequent long-lived decays into $Z\nu$, $W^\pm \ell^\mp$, or $h\nu$, and employ an inclusive search for displaced vertex signatures at the muon collider under specific benchmark parameter settings. Our results indicate strong sensitivity to the sterile neutrino parameter space, complementing other ongoing searches.

We organize the paper as follows. In section II, we describe the model with two Majorana sterile neutrinos in gauged $U(1)_{L_\mu-L_\tau}$ and their possible decay channels. In section III, we discuss the existing constraints from collider searches, neutrino trident process, and muon $g-2$ measurements. In section IV, we consider the possible production channels at the muon collider. In section V, we discuss the long-lived particle (LLP) signatures and their detection at the muon collider. In section VI, we conclude.

II. THE MODEL

To construct a UV-complete model, we extend the SM gauge group with an additional $U(1)_{L_\mu-L_\tau}$ gauge group. Additionally, we introduce a new fermion N and a complex scalar ϕ , both of which are singlets under the SM group but charged under the $U(1)_{L_\mu-L_\tau}$ gauge group. The gauge charges

of these particles are summarized in Tab. I.

Gauge Group	$L_\mu = \begin{pmatrix} \nu_{\mu,L} \\ \mu_L \end{pmatrix}$	μ_R	$L_\tau = \begin{pmatrix} \nu_{\tau,L} \\ \tau_L \end{pmatrix}$	τ_R	N	ϕ
$SU(2)_L$	2	1	2	1	1	1
$U(1)_Y$	-1	-2	-1	-2	0	0
$U(1)_{L_\mu-L_\tau}$	1	1	-1	-1	1	-2

TABLE I. Gauge charges of new particles and relevant SM particles in gauge groups.

Based on the charges of the particles under the gauge groups, the effective Lagrangian can be expressed as

$$\begin{aligned}
\mathcal{L} \supset & -\frac{1}{4}Z'_{\mu\nu}Z'^{\mu\nu} + \sum_{\alpha=\mu,\tau} \left(i\bar{L}_\alpha^0 \not{D} L_\alpha^0 + i\bar{\ell}_{\alpha,R}^0 \not{D} \ell_{\alpha,R}^0 \right) \\
& + \bar{N}^0 i\not{D} N^0 - m_N \bar{N}^0 N^0 - y' \bar{L}_\mu^0 \tilde{H} N_R^0 - y_L \phi \bar{N}_L^{0,c} N_L^0 - y_R \phi \bar{N}_R^{0,c} N_R^0 + \text{h.c.} \\
& + (D_\mu \phi)^\dagger D^\mu \phi + V(\phi),
\end{aligned} \tag{1}$$

where $Z'_{\mu\nu} = \partial_\mu Z'_\nu - \partial_\nu Z'_\mu$ is the field-strength tensor, H is the standard model Higgs doublet, the covariant derivative is given by $D_\mu = \partial_\mu - ig_Y \frac{Y}{2} B_\mu - ig_W T^i W_\mu^i - ig_{Z'} Y' Z'_\mu$, where B_μ , W_μ^i and Z'_μ represent the gauge fields for the $U(1)_Y$, $SU(2)_L$ and $U(1)_{L_\mu-L_\tau}$ groups, respectively. The constants g_Y , g_W and $g_{Z'}$ are their associated coupling constants. All fields with a superscript '0' refer to the interacting eigenstates. Furthermore, L_α and $\ell_{\alpha,R}$ represent the SM left-handed and right-handed leptons, respectively, with α denoting their flavor. It is important to note that only ν_μ couples to N_R , while ν_τ does not due to the $U(1)_{L_\mu-L_\tau}$ charge assignment.

After the electroweak and $U(1)_{L_\mu-L_\tau}$ symmetry breaking, the scalar fields are given by $H = \begin{pmatrix} 0 \\ v_h + h \end{pmatrix}$ and $\phi = v_\varphi + \varphi$, where $v_{h/\varphi}$ denotes the vacuum expectation value (vev) of the Higgs and scalar ϕ , respectively. Then the effective Lagrangian can be written as

$$\begin{aligned}
\mathcal{L}_{\text{eff}} = & \mathcal{L}_{\text{SM}} - \frac{1}{4}Z'_{\mu\nu}Z'^{\mu\nu} + \frac{1}{2}m_{Z'}^2 Z'_\mu Z'^\mu + \bar{N}^0 i\partial_\mu \gamma^\mu N^0 - m_N \bar{N}^0 N^0 \\
& + g_{Z'} Z'_\alpha (\bar{\mu} \gamma^\alpha \mu - \bar{\tau} \gamma^\alpha \tau + \bar{\nu}_{\mu,L}^0 \gamma^\alpha \nu_{\mu,L}^0 - \bar{\nu}_{\tau,L} \gamma^\alpha \nu_{\tau,L} + \bar{N}^0 \gamma^\alpha N^0) \\
& + \left(-y' \frac{(v_h + h)}{\sqrt{2}} \bar{\nu}_{\mu,L}^0 N_R^0 - y_L \frac{(v_\varphi + \varphi)}{\sqrt{2}} \bar{N}_L^{0,c} N_L^0 - y_R \frac{(v_\varphi + \varphi)}{\sqrt{2}} \bar{N}_R^{0,c} N_R^0 + \text{h.c.} \right) \\
& + \frac{1}{2} \partial_\mu \varphi \partial^\mu \varphi - \frac{1}{2} m_\varphi^2 \varphi^2 + 2v_\varphi g_{Z'}^2 Y'^2 \varphi Z'_\mu Z'^\mu + g_{Z'}^2 Y'^2 \varphi^2 Z'_\mu Z'^\mu + V_{\varphi\text{-self}},
\end{aligned} \tag{2}$$

where $m_{Z'} = 2g_{Z'}v_\varphi$, and $V_{\varphi\text{-self}}$ denotes the potential terms for the φ self-interactions. The mass terms of the above formula can be organized as

$$\mathcal{L}_{\text{mass}} \supset -\frac{1}{2}\bar{n}^{0,c}Mn^0 + \text{h.c.} = -\frac{1}{2}\bar{n}^c M_d n + \text{h.c.}, \quad (3)$$

where n denotes the mass eigenstate and n^0 represents the interaction eigenstate. For simplicity, we will later use ν_L to represent $\nu_{\mu,L}$ throughout the discussion. The complete definitions of n^0 and M are:

$$n^0 \equiv \begin{pmatrix} \nu_L^0 \\ N_L^0 \\ N_R^{0,c} \end{pmatrix}, \quad M \equiv \begin{pmatrix} 0 & 0 & m_D \\ 0 & m_L & m_N \\ m_D & m_N & m_R \end{pmatrix}, \quad (4)$$

with

$$m_D = y'v_h/\sqrt{2}, \quad m_L = \sqrt{2}y_L v_\varphi, \quad m_R = \sqrt{2}y_R v_\varphi. \quad (5)$$

The orthogonal matrix U can be used to diagonalize the mass matrix, achieving $U^T M U = M_d$, and $n = U^T n^0$. We assume the mass hierarchy $m_R \gg m_L, m_D, m_N$, the mass matrix M can be diagonalized to the leading order in m_R^{-1} as follows,

$$M_d = \begin{pmatrix} -\frac{m_D^2}{m_R} & 0 & 0 \\ 0 & m_L - \frac{m_N^2}{m_R} & 0 \\ 0 & 0 & m_R + \frac{m_D^2 + m_N^2}{m_R} \end{pmatrix} + \mathcal{O}(m_R^{-2}). \quad (6)$$

If we define the mixing angles

$$\theta_N \equiv \frac{m_N}{m_R}, \quad \theta_{\nu R} \equiv \frac{m_D}{m_R}, \quad \theta_{\nu L} \equiv \frac{m_N}{m_L} \frac{m_D}{m_R} = \frac{m_N}{m_L} \theta_{\nu R}, \quad (7)$$

where θ_N representing N_L - N_R mixing, $\theta_{\nu R}$ representing active ν - N_R mixing and $\theta_{\nu L}$ representing active ν - N_L mixing. The orthogonal matrix can be simplified by expanding in terms of m_R^{-1} ,

$$U \simeq \begin{pmatrix} 1 & -\theta_{\nu L} & \theta_{\nu R} \\ \theta_{\nu L} & 1 & \theta_N \\ -\theta_{\nu R} & -\theta_N & 1 \end{pmatrix} - \begin{pmatrix} \frac{1}{2}(\theta_{\nu L}^2 + \theta_{\nu R}^2) & \theta_N \theta_{\nu R} \left(1 - \frac{\theta_{\nu L}^2}{\theta_N^2} + \frac{\theta_{\nu L}^2}{\theta_{\nu R}^2}\right) & 0 \\ \theta_{\nu L}^2 \left(\frac{\theta_{\nu R}}{\theta_N} - \frac{\theta_N}{\theta_{\nu R}}\right) & \frac{1}{2}(\theta_N^2 + \theta_{\nu L}^2) & -\theta_N^2 \frac{\theta_{\nu R}}{\theta_{\nu L}} \\ \theta_N \theta_{\nu L} & \theta_N^2 \left(\frac{\theta_{\nu R}}{\theta_{\nu L}} - \frac{\theta_{\nu L} \theta_{\nu R}}{\theta_N^2}\right) & \frac{1}{2}(\theta_N^2 + \theta_{\nu R}^2) \end{pmatrix} + \mathcal{O}(m_R^{-3}). \quad (8)$$

We retain U up to the order of $\mathcal{O}(m_R^{-2})$ while deriving the interaction terms of the Lagrangian, as there is a cancellation at the order of $\mathcal{O}(m_R^{-1})$ in deriving Eq. (16) for the $Z' - N_L - \nu_L$ vertex. From the mass matrix M_d above, the masses of the light active neutrino and the two heavy Majorana sterile neutrinos can be derived as

$$\begin{aligned} m_\nu \equiv m_1 &\simeq \frac{m_D^2}{m_R} = m_R \theta_{\nu R}^2, \\ m_2 &= m_L - \frac{m_N^2}{m_R} \simeq m_L, \\ m_3 &= m_R + \frac{m_D^2 + m_N^2}{m_R} \simeq m_R, \end{aligned} \quad (9)$$

with the mass hierarchy $m_\nu \ll m_2 \ll m_3$. Due to the approximate equality, we continue using m_L and m_R to represent the physical masses of N_L and N_R , respectively. The minus sign of active neutrino mass has been eliminated by redefining the neutrino field phase. It is important to note that the right-handed sterile neutrino plays a key role in imparting mass to the active neutrino, consistent with the typical seesaw mechanism. In contrast, the left-handed sterile neutrino does not directly contribute to neutrino mass generation. Since neutrino mass is related to m_D and m_R , these parameters can be fixed by the neutrino mass m_ν and mixing angle $\theta_{\nu R}$:

$$m_R = \frac{m_\nu}{\theta_{\nu R}^2}, \quad m_D = \frac{m_\nu}{\theta_{\nu R}}. \quad (10)$$

Additionally, the parameters θ_N and m_N can be determined by:

$$m_N = \frac{m_L \theta_{\nu L}}{\theta_{\nu R}}, \quad \theta_N = \frac{m_L \theta_{\nu L}}{m_R \theta_{\nu R}}. \quad (11)$$

Thus, this model has the following relevant parameters:

$$\{g_{Z'}, m_{Z'}, m_\varphi, m_L, \theta_{\nu L}, \theta_{\nu R}\} \quad (12)$$

To achieve a small active neutrino mass, $m_\nu = \frac{m_D^2}{m_R}$, without fine-tuning the Higgs Yukawa coupling in the term $(y' \bar{L}_\mu^0 \tilde{H} N_R^0)$, we impose the following requirements:

$$m_\nu \simeq \mathcal{O}(0.1) \text{ eV}, \quad m_D \gtrsim 1 \text{ MeV}, \quad (13)$$

therefore, the m_R should be larger than 10 TeV. In our study, we focus primarily on the left-handed sterile neutrino N_L at a muon collider with $\sqrt{s} = 3$ or 10 TeV. A heavy m_R implies a correspondingly large v_φ , due to the $O(1)$ Yukawa coupling y_R between φ and N_R . To prevent the on-shell production of N_R and φ at the muon collider, we assume that both m_φ and m_R (e.g. $m_R = 100$ TeV) are significantly heavier than the collider's center-of-mass energy. Thus, we could assume N_R and φ are effectively decoupled and $\theta_{\nu R}$ will be fixed by the neutrino mass. With these in mind, the free parameters of this model will be reduced to fours:

$$\{g_{Z'}, m_{Z'}, m_L, \theta_{\nu L}\}. \quad (14)$$

Next, we will consider the Lagrangian in the mass eigenstates. We will decompose interaction terms of the Lagrangian into two parts: gauge interactions and scalar interactions.

$$\mathcal{L}_{\text{int}} \supset \mathcal{L}_{\text{gauge}} + \mathcal{L}_{\text{scalar}}, \quad (15)$$

where the gauge Lagrangian related to the neutrino can be expanded in terms of m_R^{-1} to the leading order, considering that m_R is very large

$$\begin{aligned} \mathcal{L}_{\text{gauge}} \supset & \left(\frac{g_W}{\sqrt{2}} \bar{\nu}_L^0 W \mu_L^0 + \text{h.c.} \right) + \frac{g_W}{2 \cos \theta_W} \bar{\nu}_L^0 Z \nu_L^0 \\ & + g_{Z'} Z'_\mu \left(\bar{\mu} \gamma^\mu \mu + \bar{\nu}_L^0 \gamma^\mu \nu_L^0 + \bar{N}_L^0 \gamma^\mu N_L^0 - \bar{N}_R^{0,c} \gamma^\mu N_R^{0,c} \right) \\ \simeq & \frac{g_W}{\sqrt{2}} W_\mu \left(\bar{\nu}_L \gamma^\mu \mu_L + \theta_{\nu R} \bar{N}_R^c \gamma^\mu \mu_L - \theta_{\nu L} \bar{N}_L \gamma^\mu \mu_L + \text{h.c.} \right) \\ & + \frac{g_W}{2 \cos \theta_W} Z_\mu \left[\bar{\nu}_L \gamma^\mu \nu_L + \theta_{\nu L}^2 \bar{N}_L \gamma^\mu N_L + \theta_{\nu R}^2 \bar{N}_R^c \gamma^\mu N_R^c \right. \\ & \left. + \left(\theta_{\nu R} \bar{\nu}_L \gamma^\mu N_R^c - \theta_{\nu L} \bar{\nu}_L \gamma^\mu N_L - \theta_{\nu L} \theta_{\nu R} \bar{N}_L \gamma^\mu N_R^c + \text{h.c.} \right) \right] \\ & + g_{Z'} Z'_\mu \left[\bar{\mu} \gamma^\mu \mu + \bar{\nu}_L \gamma^\mu \nu_L + \bar{N}_L \gamma^\mu N_L - \bar{N}_R^c \gamma^\mu N_R^c \right. \\ & \left. + \left(2\theta_{\nu R} \bar{\nu}_L \gamma^\mu N_R^c + 2\theta_{\nu L} \bar{N}_L \gamma^\mu N_R^c - 2\theta_{\nu L} \theta_{\nu R} \bar{\nu}_L \gamma^\mu N_L + \text{h.c.} \right) \right]. \end{aligned} \quad (16)$$

From the above Lagrangian, the mixing of N_L with the active neutrino, characterized by the angle $\theta_{\nu L}$, can be quite small due to the two-step mixing process: $N_L \rightarrow N_R^c \rightarrow \nu_L$. As a result, N_L has the potential to be a long-lived particle at the muon collider. Also, the interactions relevant to the

SM Higgs and φ are reduced to

$$\begin{aligned}
\mathcal{L}_{\text{scalar}} \supset & -\frac{m_R \theta_{\nu R}}{v_h} h \left(\bar{\nu}_L N_R - \theta_{\nu R} \bar{\nu}_L \nu_L^c - \theta_N \bar{\nu}_L N_L^c - \theta_{\nu L} \bar{N}_L N_R + \theta_N \theta_{\nu L} \bar{N}_L N_L^c + \theta_{\nu R} \bar{N}_R^c N_R + \text{h.c.} \right) \\
& -\frac{\varphi}{2v_\varphi} \left[m_L \left(\bar{N}_L^c N_L + 2\theta_{\nu L} \bar{\nu}_L^c N_L + 2\theta_N \bar{N}_L^c N_R^c \right) + m_R \left(\bar{N}_R^c N_R - 2\theta_{\nu R} \bar{\nu}_L^c N_R^c - 2\theta_N \bar{N}_L^c N_R^c \right) + \text{h.c.} \right] \\
& + \frac{1}{2} \partial_\mu \varphi \partial^\mu \varphi - \frac{1}{2} m_\varphi^2 \varphi^2 + 2v_\varphi g_{Z'}^2 Y'^2 \varphi Z'_\mu Z'^\mu + g_{Z'}^2 Y'^2 \varphi^2 Z'_\mu Z'^\mu + \mathcal{L}_{\varphi\text{-self}}.
\end{aligned} \tag{17}$$

In the above Lagrangian, we omit the full expression of $\mathcal{L}_{\varphi\text{-self}}$ since we assume that φ is too heavy to be produced at the muon collider. Given the center-of-mass energy of the collider, $\sqrt{s} = 3$ or 10 TeV, searching for the on-shell production of N_R is also not feasible. The final relevant interaction terms of the Lagrangian related to ν_L and N_L , up to order m_R^{-1} , can be written as:

$$\begin{aligned}
\mathcal{L}_{\text{int}} \supset & \frac{g_W}{\sqrt{2}} W_\mu \left(\bar{\nu}_L \gamma^\mu \mu_L - \theta_{\nu L} \bar{N}_L \gamma^\mu \mu_L + \text{h.c.} \right) \\
& + \frac{g_W}{2 \cos \theta_W} Z_\mu \left(\bar{\nu}_L \gamma^\mu \nu_L - \theta_{\nu L} \bar{\nu}_L \gamma^\mu N_L + \text{h.c.} \right) \\
& + g_{Z'} Z'_\mu \left(\bar{\mu} \gamma^\mu \mu + \bar{\nu}_L \gamma^\mu \nu_L + \bar{N}_L \gamma^\mu N_L \right) \\
& + \left(\frac{m_\nu}{v_h} h \bar{\nu}_L \nu_L^c + \frac{m_L \theta_{\nu L}}{v_h} h \bar{\nu}_L N_L^c + \text{h.c.} \right).
\end{aligned} \tag{18}$$

The partial decay widths of N_L based on above Lagrangian in the limit $m_\ell \rightarrow 0$ are [82]:

$$\begin{aligned}
\Gamma(N_L \rightarrow \mu^- W^+) &= \Gamma(N_L \rightarrow \mu^+ W^-) = \frac{\theta_{\nu L}^2 g_W^2 (m_L^2 - m_W^2)^2 (m_L^2 + 2m_W^2)}{64\pi m_L^3 m_W^2}, \\
\Gamma(N_L \rightarrow \nu_\mu Z) &= \frac{\theta_{\nu L}^2 g_W^2 (m_L^2 - m_Z^2)^2 (m_L^2 + 2m_Z^2)}{128\pi m_L^3 m_W^2}, \\
\Gamma(N_L \rightarrow \nu_\mu h) &= \frac{\theta_{\nu L}^2 g_W^2 (m_L^2 - m_h^2)^2}{128\pi m_L m_W^2}, \\
\Gamma_{N_L} &= 2\Gamma(N_L \rightarrow \mu^\pm W^\mp) + \Gamma(N_L \rightarrow \nu_\mu Z) + \Gamma(N_L \rightarrow \nu_\mu h),
\end{aligned} \tag{19}$$

where Γ_{N_L} is the total decay width of N_L . In the large m_L limit, the decay width of N_L is proportional to $\theta_{\nu L}^2 m_L^3 / v_h^2$. The branching ratios of N_L are shown in the left panel of Fig. 1, where the one labeled by $\mu^\pm W^\mp$ means the sum of the two charge-conjugated channels, $N_L \rightarrow \mu^+ W^-$ and $N_L \rightarrow \mu^- W^+$. We focus on N_L with masses greater than 100 GeV, which is the region of interest. When m_L is significantly larger than the Higgs mass, the branching ratios of N_L are approximate: $N_L \rightarrow \mu^\pm W^\mp$ at 66%, $N_L \rightarrow \nu_\mu Z$ at 17%, and $N_L \rightarrow \nu_\mu h$ at 17%. Need to mention that the total width of N_L also

can be transformed into $\Gamma_{N_L} \propto m_\nu (m_L/m_R) (m_N^2/v_h^2)$. Therefore, we explicitly see the width of N_L is suppressed by small active neutrino mass m_ν , and the small Dirac mass of sterile neutrinos.

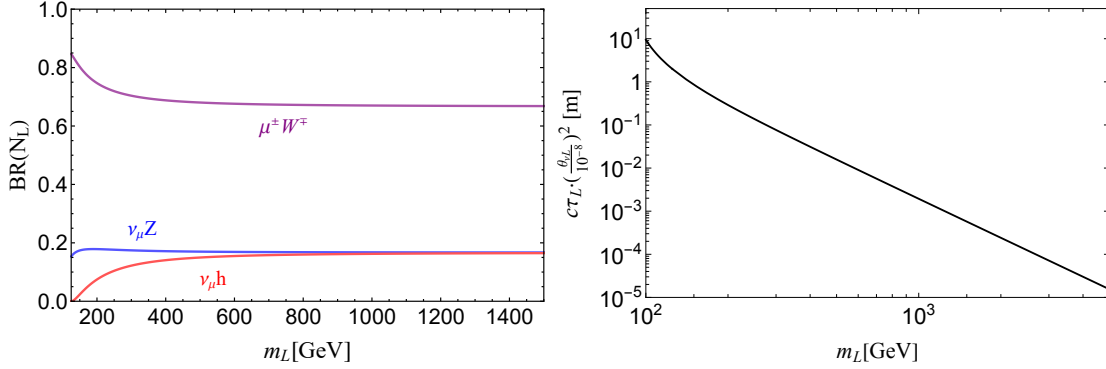


FIG. 1. The branching ratios of sterile neutrino N_L decay (left) and its proper decay length (right) as a function of sterile neutrino mass m_L . The three main decay branching ratios are shown in different colors with purple corresponding to $N_L \rightarrow \mu^\pm W^\mp$, blue corresponding to $N_L \rightarrow \nu_\mu Z$, and red corresponding to $N_L \rightarrow \nu_\mu h$.

When $m_L \gg m_W, m_Z, m_h$, all decay channels of N_L are open, and the sterile neutrino's proper decay length $c\tau_L$ can be directly obtained from the total decay width of N_L :

$$c\tau_L = \frac{1}{\Gamma_{N_L}} \simeq 2 \text{ m} \times \left(\frac{10^{-8}}{\theta_{\nu L}} \right)^2 \left(\frac{100 \text{ GeV}}{m_L} \right)^3, \quad (20)$$

where $g_W = 0.65$, $m_W = 80.4 \text{ GeV}$, and c is the speed of light. The dependence of the lifetime on m_L is illustrated in the right panel of Fig. 1, where the complete formula for $c\tau_L = 1/\Gamma_{N_L}$ from Eq. (19) is used. In the relevant parameter space, for example, with $\theta_{\nu L} = 10^{-8}$ and $m_L = 100 \text{ GeV}$, the sterile neutrino N_L has a proper decay length of approximately 9.4 meters, because the decay channel $N_L \rightarrow h\nu_\mu$ is forbidden and must be excluded from the calculation. This long-lived signature could potentially be observed at future muon colliders.

III. CONSTRAINTS

In this section, we discuss the constraints on our model. Regarding collider searches for HNLs at the LHC, two types of searches apply. Long-lived HNL searches, which target N_L than the gauge bosons in the SM, do not constrain our model since we focus on $m_L > 100 \text{ GeV}$ [35, 41]. Searches for heavier HNLs N_R , primarily produced through W-boson s-channel processes, the constraint on

the mixing angles between active neutrino and sterile neutrino is 10^{-2} [83–86], which are outside our region of interest ($\theta_{\nu L} < 10^{-6}$). Therefore, we neglect LHC constraints in this discussion.

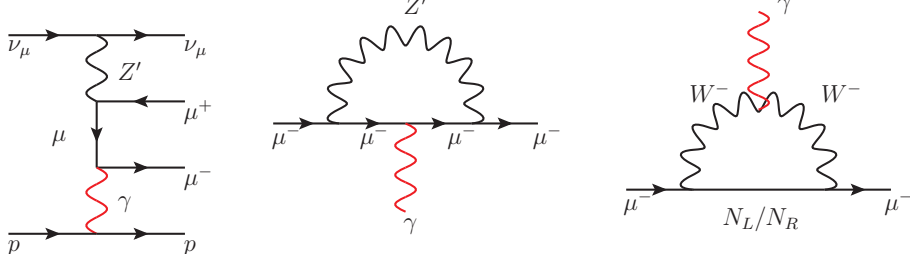


FIG. 2. Feynman diagrams of relevant constraint processes for our model. The left panel represents the neutrino trident process, and the middle and right one correspond to the lepton magnetic dipole process.

The $U(1)_{L_\mu-L_\tau}$ symmetry imposes natural limits from well-known measurements of the neutrino trident process [87], as shown in the left panel of Fig. 2. Introducing a new gauge boson and sterile neutrinos also affects the muon magnetic moment anomaly, depicted in the right panels of Fig. 2. We will focus on the constraints from neutrino trident process measurements and the muon magnetic moment anomaly.

The relevant muon-neutrino trident process, illustrated in the left panel of Fig. 2, is given by:

$$\nu_\mu N \rightarrow \nu_\mu N \mu^+ \mu^-, \quad (21)$$

where N represents the nucleus. In our model, the primary contribution to this process comes from the Z' boson. In the heavy mass limit of $m_{Z'} \gg \sqrt{s}$, the total cross section can be expressed as [88]:

$$\sigma(\text{SM} + Z') \approx \frac{1 + \left(1 + 4 \sin^2 \theta_W + 2 \frac{v_h^2}{(m_{Z'}/g_{Z'})^2}\right)^2}{1 + (1 + 4 \sin^2 \theta_W)^2} \sigma(\text{SM}), \quad (22)$$

where $\sigma(\text{SM})$ is the SM cross section [87]. The inclusive neutrino trident production cross section, $\sigma(\nu_\mu N \rightarrow \nu_\mu N \mu^+ \mu^-)$, measured by the CCFR collaboration, agrees well with SM predictions, yielding [89]:

$$\sigma/\sigma_{\text{SM}} = 0.82 \pm 0.28. \quad (23)$$

Combining the experimental results with theoretical predictions, we obtain the following upper limit (at 95% C.L.) on the parameters $g_{Z'}$ and $m_{Z'}$:

$$\frac{g_{Z'}}{m_{Z'}} < 1.86 \times 10^{-3} \text{ GeV}^{-1}. \quad (24)$$

This constraint implies that the vev v_ϕ must exceed $2.69 \times 10^2 \text{ GeV}$ if $m_{Z'} = 2g_{Z'}v_\phi$. Therefore, the neutrino trident constraints reinforce our earlier assumption of a large m_R and the decoupling of the heavy ϕ and N_R particles.

Another significant constraint comes from the measurement of the muon anomalous magnetic moment $g - 2$, which requires $\Delta a_\mu = (249 \pm 48) \times 10^{-11}$ [90, 91]. In our framework, the primary contributions to the muon magnetic moment arise from the one-loop diagram involving the $U(1)_{L_\mu-L_\tau}$ gauge boson Z' (middle panel of Fig. 2) and the two sterile neutrinos N_L and N_R (right panel of Fig. 2). To leading order, the contributions from the Z' and sterile neutrino processes can be derived as [92]:

$$\begin{aligned} \Delta a_\mu(Z') &= \frac{g_{Z'}^2 m_\mu^2}{4\pi^2 m_{Z'}^2} \int_0^1 \frac{x^2(1-x)}{1-x+x^2 \frac{m_\mu^2}{m_{Z'}^2}} dx, \\ \Delta a_\mu(N_L) &= \frac{\theta_{\nu L}^2 g_W^2 m_\mu^2}{32\pi^2 m_W^2} \int_0^1 \frac{2x^2(1+x) + \frac{m_L^2}{m_W^2}(2x-3x^2+x^3)}{x + \frac{m_L^2}{m_W^2}(1-x)} dx, \\ \Delta a_\mu(N_R) &= \Delta a_\mu(N_L)(m_L \rightarrow m_R, \theta_{\nu L} \rightarrow \theta_{\nu R}). \end{aligned} \quad (25)$$

In the limits $m_{Z'} \gg m_\mu$ and $m_L, m_R \gg m_W$, these formulas can be simplified to:

$$\begin{aligned} \Delta a_\mu(Z') &\simeq \frac{g_{Z'}^2 m_\mu^2}{12\pi^2 m_{Z'}^2}, \\ \Delta a_\mu(N_L) &\simeq \frac{G_F}{\sqrt{2}} \frac{\theta_{\nu L}^2 m_\mu^2}{8\pi^2} f\left(\frac{m_L^2}{m_W^2}\right), \\ \Delta a_\mu(N_R) &\simeq \frac{G_F}{\sqrt{2}} \frac{\theta_{\nu R}^2 m_\mu^2}{8\pi^2} f\left(\frac{m_R^2}{m_W^2}\right), \end{aligned} \quad (26)$$

where $f(r)$ is given by

$$f(r) = \frac{10 - 43r + 78r^2 - 49r^3 + 4r^4 + 18r^3 \ln(r)}{3(1-r)^4}. \quad (27)$$

Given that $g_{Z'} \gg \theta_{\nu L}, \theta_{\nu R}$ and $m_L, m_R \gg m_\mu, m_W$, the dominant contribution to the muon $g - 2$ comes from the Z' . This places an upper limit on the parameters $g_{Z'}$ and $m_{Z'}$, constraining the model to ensure compatibility with the observed muon magnetic moment anomaly. By requiring that the main $g - 2$ contribution from the Z' process (the first line of Eq. (26)) be smaller than $\Delta a_\mu = (249 + 2 \times 48) \times 10^{-11}$, consistent with the experimental constraint, we can derive the upper bound on the parameters $g_{Z'}$ and $m_{Z'}$ under the assumption that $m_{Z'} \gg m_\mu$:

$$\frac{g_{Z'}}{m_{Z'}} \lesssim 6.09 \times 10^{-3} \text{ GeV}^{-1}. \quad (28)$$

Comparing with Eq. (24), we can see that the constraint from the muon $g - 2$ is weaker than that from the neutrino trident experiments.

IV. PRODUCTION AT FUTURE MUON COLLIDER

In this section, we will investigate the phenomenology of the sterile neutrino N_L at a future high-energy muon collider. Following the collider settings outlined in Ref. [56], we consider two benchmark scenarios: one with a center-of-mass energy $\sqrt{s} = 3 \text{ TeV}$ and an integrated luminosity $\mathcal{L} = 1 \text{ ab}^{-1}$; and the other with $\sqrt{s} = 10 \text{ TeV}$ and $\mathcal{L} = 10 \text{ ab}^{-1}$.

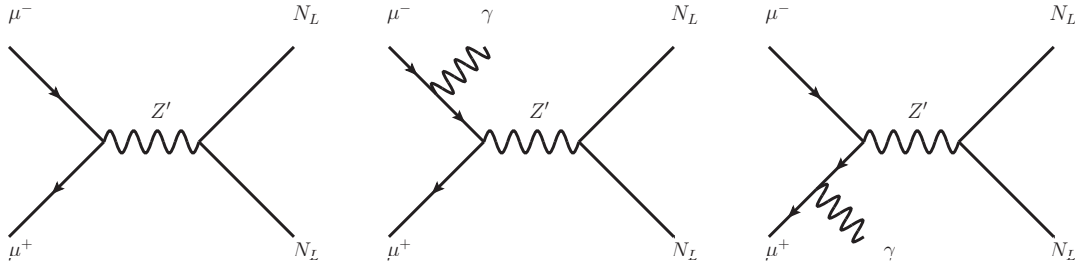


FIG. 3. The Feynman diagrams for the production processes of sterile neutrino N_L at the muon collider. The left panel shows the direct pair production mediated by Z' , $\mu^+\mu^- \rightarrow N_L N_L$. The middle and the right panels show the production process with an initial radiated photon, $\mu^+\mu^- \rightarrow N_L N_L \gamma$.

The sterile neutrino N_L can be produced at a muon collider through two main channels based on the interaction of Eq. (18), as depicted in Fig. 3. The first production mechanism, shown in the left panel, involves direct pair production of N_L mediated by Z' . The second, shown in the right two panels, involves an initial radiated photon.

The pair production of heavy neutral leptons N_L via a Z' boson can occur whenever the $\sqrt{s} >$

$2m_L$. The cross section for this process is given by:

$$\sigma(\mu^+\mu^-\rightarrow N_L N_L) = \frac{g_{Z'}^4 s}{24\pi((s-m_{Z'}^2)^2+m_{Z'}^2\Gamma_{Z'}^2)} \left(1-\frac{4m_L^2}{s}\right)^{\frac{3}{2}}, \quad (29)$$

where $\Gamma_{Z'}$ is the total decay width of Z' , accounting for all possible decay channels, which can be written as:

$$\Gamma_{Z'} = \frac{g_{Z'}^2}{12\pi m_{Z'}} \left(\sum_{\ell=\mu,\tau} (m_{Z'}^2+2m_\ell^2) \sqrt{1-\frac{4m_\ell^2}{m_{Z'}^2}} + \sum_{\ell=\nu_\mu,\nu_\tau} \frac{1}{2} (m_{Z'}^2-4m_\ell^2) \sqrt{1-\frac{4m_\ell^2}{m_{Z'}^2}} + \frac{1}{2} (m_{Z'}^2-4m_L^2) \theta(m_{Z'}-2m_L) \sqrt{1-\frac{4m_L^2}{m_{Z'}^2}} \right), \quad (30)$$

where the first term represents the decay channels for $Z' \rightarrow \mu^-\mu^+$ and $Z' \rightarrow \tau^-\tau^+$, the second term refers to the channels for $Z' \rightarrow \nu_\mu\bar{\nu}_\mu$ and $Z' \rightarrow \nu_\tau\bar{\nu}_\tau$, and the last term corresponds to the channel for $Z' \rightarrow N_L N_L$. Here $\theta(x)$ is the Heaviside step function, which equals 1 for $x > 0$ and 0 otherwise. We show the branching ratios of Z' in Fig. 4 focusing on the case where $m_L > 100$ GeV. The decay channel $Z' \rightarrow N_L N_L$ appears when the mass satisfy $m_{Z'} > 2m_L$. When Z' is much heavier than $2m_L$, the branching ratio among these three channels will satisfy the relation $\text{BR}(Z' \rightarrow \ell\ell) : \text{BR}(Z' \rightarrow \nu\nu) : \text{BR}(Z' \rightarrow N_L N_L) \simeq 4 : 2 : 1$. If $m_{Z'} < 2m_L$, the branching ratio will satisfy $\text{BR}(Z' \rightarrow \ell\ell) : \text{BR}(Z' \rightarrow \nu\nu) : \text{BR}(Z' \rightarrow N_L N_L) \simeq 4 : 2 : 0$.

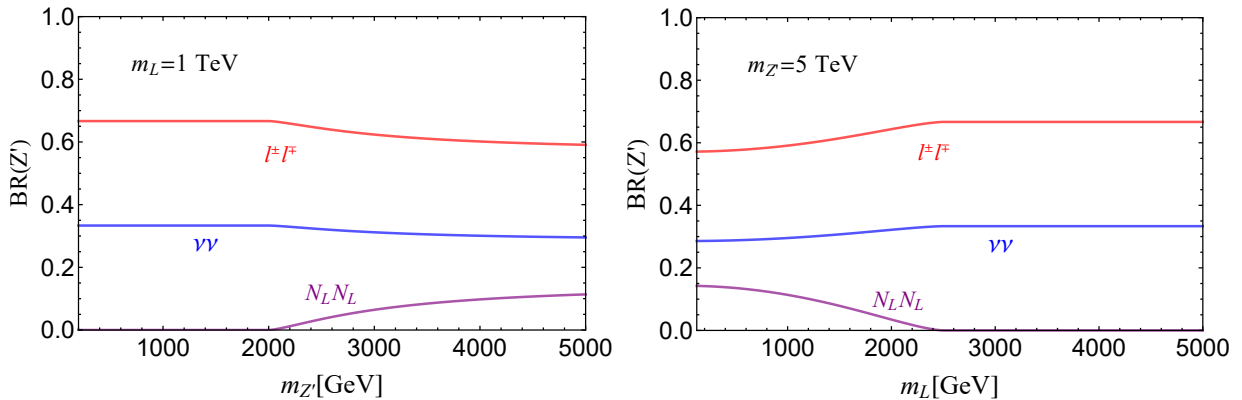


FIG. 4. The branching ratios of Z' decays as a function of $m_{Z'}$ (left) and m_L (right). The left (right) panel shows the case with $m_L = 1 \text{ TeV}$ ($m_{Z'} = 5 \text{ TeV}$), where the red line, blue line, and purple line correspond to the decay channels to charged leptons, neutrinos, and sterile neutrino, respectively.

For the production process $\mu^+\mu^- \rightarrow Z'^{(*)}\gamma \rightarrow N_L N_L \gamma$ (the middle and right panel of Fig. 3) this

also can occur whenever $\sqrt{s} > 2m_L$. The Z' can be either on-shell or off-shell depending on the mass of Z' . For $\sqrt{s} > m_{Z'}$, Z' can be produced on-shell associated with initial state radiation, which leads to two-body final state $\mu^+\mu^- \rightarrow Z'\gamma$ followed by further decay $Z' \rightarrow N_L N_L$ when $m_{Z'} > 2m_L$. The cross section in this case can be approximated using the narrow width approximation:

$$\sigma(\mu^+\mu^- \rightarrow N_L N_L \gamma) \approx \sigma(\mu^+\mu^- \rightarrow Z'\gamma) \cdot \text{BR}(Z' \rightarrow N_L N_L), \quad (31)$$

where the differential cross section for $Z'\gamma$ production can be calculated as:

$$\frac{d\sigma}{d\cos\theta}(\mu^+\mu^- \rightarrow Z'\gamma) = \frac{\alpha g_{Z'}^2 (1 - m_{Z'}^2/s)}{2s \sin^2\theta} \left(1 + \cos^2\theta + \frac{4sm_{Z'}^2}{(s - m_{Z'}^2)^2} \right), \quad (32)$$

where θ represents the Z' scattering angle with respect to the beam line, and the muon mass is ignored. The differential cross section diverges at $\theta \rightarrow 0$ and π , thus we need the cut on θ to get a finite cross section. After considering the relationship between the θ and the pseudorapidity. In next section for the collider simulation, we choose $p_T^\gamma > 20$ GeV and $|\eta_\gamma| < 2.5$ to remove the beam-induced backgrounds typically present at muon colliders. Such pseudorapidity cut implies $\theta \approx 10^\circ$ (170°), so we choose the integration cut off for the cross section as $\theta \approx 10^\circ$ (170°). For the parameter choice, $g_{Z'} = 0.1$, $m_{Z'} = 2$ TeV, and $\sqrt{s} = 3$ TeV, the cross section is evaluated as $\sigma(\mu^+\mu^- \rightarrow Z'\gamma) \approx 32.6$ fb. It should be noted that these cross sections were computed numerically using MadGraph 5 [93], and are consistent with analytical results of Eq. (31).

For $m_{Z'} > \sqrt{s}$, the two-body production $\mu^+\mu^- \rightarrow Z'\gamma$ is kinematically forbidden. In this case, the only viable process is the three-body production $\mu^+\mu^- \rightarrow Z'^{(*)}\gamma \rightarrow N_L N_L \gamma$, mediated by an off-shell Z' . To account for this contribution, we used MadGraph 5 to numerically compute the corresponding cross section.

In order to understand which process is dominant, we show the production cross section in Fig. 5 with $g_{Z'} = 0.1$, choosing two benchmark center-of-mass energy $\sqrt{s} = 3$ TeV and $\sqrt{s} = 10$ TeV, respectively. We consider three benchmark values of $m_{Z'}$ for each center-of-mass energy: $m_{Z'} = 2$ TeV, $m_{Z'} = 3$ TeV, and $m_{Z'} = 5$ TeV for $\sqrt{s} = 3$ TeV; $m_{Z'} = 8$ TeV, $m_{Z'} = 10$ TeV, and $m_{Z'} = 12$ TeV for $\sqrt{s} = 10$ TeV. The solid lines represent the pair production process $\mu^-\mu^+ \rightarrow N_L N_L$, while the dashed lines indicate the initial state radiation process $\mu^+\mu^- \rightarrow N_L N_L \gamma$, which include both Z' on-shell and off-shell. Compare the left and right panels in Fig. 5, when $m_{Z'} \approx \sqrt{s}$, the total cross section is enhanced, but the $N_L N_L$ process will be enhanced more than the $N_L N_L \gamma$

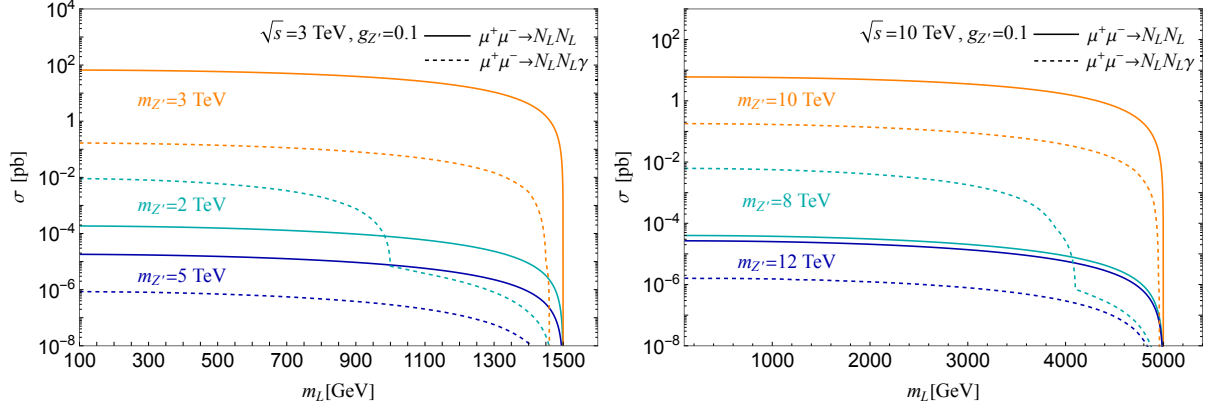


FIG. 5. The cross sections for pair production of sterile neutrino N_L are plotted with different center-of-mass energy in the left and the right panels. In each panel, the solid line represents the cross section for the direct production process $\mu^+\mu^- \rightarrow N_L N_L$, while the dashed line represents the cross section for the production with initial state radiation $\mu^+\mu^- \rightarrow N_L N_L \gamma$. Different masses of Z' are shown in different colors. Besides, the cross section for $\mu^+\mu^- \rightarrow N_L N_L$ ($\mu^+\mu^- \rightarrow N_L N_L \gamma$) with an on-shell Z' is proportional to $g_{Z'}^2$, while the one for $\mu^+\mu^- \rightarrow N_L N_L$ ($\mu^+\mu^- \rightarrow N_L N_L \gamma$) with an off-shell Z' is proportional to $g_{Z'}^4$, which shows a different scaling behavior with respect to $g_{Z'}$.

process, as seen from the comparison of the orange lines with other lines in each plot. If $m_{Z'} < \sqrt{s}$ and $m_{Z'} > 2m_L$, the production process with initial state radiation will be dominant. Conversely, if $m_{Z'} > \sqrt{s}$, or $m_{Z'} < 2m_L$, the pair production of $N_L N_L$ will be dominant because of the kinematic constraints. In our study, the cross section for $N_L N_L \gamma$ with off-shell Z' is also provided, and we include all processes to perform the inclusive analysis.

V. LONG-LIVED STERILE NEUTRINO SIGNALS AT MUON COLLIDER

At the future muon collider, after the pair production of the sterile neutrino N_L , including both $N_L N_L$ and $N_L N_L \gamma$, N_L can further decay into μW , νZ , and νh . With decay widths suppressed by the mixing angle $\theta_{\nu L}$, its proper decay length can be in the meter scale, as shown in Fig. 1. What's more, in the real decay case in the collider, the Lorentz boost factor needs to be taken into account, which makes it testable at lepton colliders through the observation of displaced vertices (DVs).

Because the branching ratio of $N_L \rightarrow \mu W$ is significantly higher than that of the other two channels, which is shown in Fig. 1, we focus on the processes N_L decays to μW , and we conduct the inclusive search strategy which requires at least one of the sterile neutrinos to decay inside the

designated detector volume. The complete signal process is :

$$\mu^+ \mu^- \rightarrow (\gamma) N_L N_L, N_L \rightarrow W^\pm \mu^\mp, W^\pm \rightarrow jj. \quad (33)$$

The number of signal events at the muon collider can be expressed as:

$$N = \mathcal{L} \cdot \sigma \cdot \langle \mathbb{P} \cdot \epsilon \rangle, \quad (34)$$

where σ is the cross section for the process Eq. (33), and ϵ is the kinematical cut efficiency and \mathbb{P} is the probability for one N_L decaying within the designated detector volume. $\langle \mathbb{P} \cdot \epsilon \rangle$ denotes the averaged inclusive efficiency, which can be calculated event-by-event at the parton level.

Parameter	$\sqrt{s} = 3 \text{ TeV}$	$\sqrt{s} = 10 \text{ TeV}$
Beam momentum [GeV]	1500	5000
Integrated luminosity [ab^{-1}]	1	10
Subsystem	R dimensions [cm]	$ Z $ dimensions [cm]
Vertex Detector Barrel	3.0 - 10.4	65.0
Inner Tracker Barrel	12.7 - 55.4	48.2 - 69.2
Outer Tracker Barrel	81.9 - 148.6	124.9

TABLE II. The muon collider operating scenarios and boundary dimensions of its tracking detector [94].

In order to numerically calculate the efficiencies, we first generate the UFO model using FeynRules [95] based on the sterile neutrino scenario in the $U(1)_{L_\mu - L_\tau}$ gauge field, as described in Sec. II. Then we simulate signal events at the parton level using MadGraph 5 [93], by inputting the UFO model. And then the parton level events are passed to the Pythia8 [96] and Delphes [97] to generate the showering, hadronization, and detector effects by using the CMS card.

Additionally, the relevant parameters for the muon collider are provided in Tab. II. For a given parton-level event, the probability \mathbb{P} that a long-lived particle (N_L) decays within the range $[r_1 \cdot \hat{\mathbf{r}}, r_2 \cdot \hat{\mathbf{r}}]$ along its flight direction $\hat{\mathbf{r}}$ is given by [98]:

$$\mathbb{P} = \exp\left(-\frac{r_1}{\gamma\beta c\tau_L}\right) - \exp\left(-\frac{r_2}{\gamma\beta c\tau_L}\right), \quad (35)$$

where γ is the Lorentz factor of the sterile neutrino N_L , β is its speed along the $\hat{\mathbf{r}}$ direction, and τ_L is its proper lifetime.

We require the sterile neutrino's displaced distance d_L along its movement direction $\hat{\mathbf{r}}$ to satisfy

$10 \text{ cm} < |d_L \cdot \sin \alpha| < 81.9 \text{ cm}$, where α is the angle between the sterile neutrino N_L 's momentum direction and the beamline axis. This minimum displacement distance requirement effectively suppresses the SM backgrounds from prompt decays, while the maximum distance requirement ensures a good track reconstruction efficiency, as shown in Tab. II. More precisely, the long-lived sterile neutrinos must decay before reaching the ‘‘Outer Tracker Barrel’’, leaving several layers for efficient reconstruction of charged particle tracks. Besides, to further depress the SM background, we also require the invariant mass of reconstructed jets to be around the W boson mass region. With other kinematic requirements, the whole selection criteria can be organized as [94]

$$\begin{aligned}
\text{DV} : \quad & p_T^\mu > 20 \text{ GeV}, |\eta_\mu| < 2.5, p_T^j > 20 \text{ GeV}, |\eta_j| < 2.5, \\
& 10 \text{ cm} < |d_L \cdot \sin \alpha| < 81.9 \text{ cm}, |d_L \cdot \cos \alpha| < 1.25 \text{ m}, \\
& m_{jj} (m_j^{\text{fat}}) \in [50, 100] \text{ GeV},
\end{aligned} \tag{36}$$

where the particles appearing are required to be well recognized and reconstructed in the Delphes, p_T and η are the transverse momentum and pseudorapidity of the muon from N_L decay or the jets from W decay, respectively, to facilitate their identification. $m_{jj} (m_j^{\text{fat}})$ is the invariant mass of the final hard jets (or fat jet [99]) from W boson decays, where the one closest to the W boson mass is adopted. Since the analysis is performed at the detector level, the isolation between muons and jets is automatically accounted for by the simulation. If the W boson is reconstructed from two hard jets, we require both jets to satisfy the p_T, η criteria.

The above selection criteria allow the DVs to be well identified, and give negligible SM backgrounds. Exactly speaking, now that the displaced vertex of the signal is reconstructed via a well-reconstructed muon and one (two) fat (energetic) jet(s). With energetic well-reconstructed displaced muon tagging, the main possible SM backgrounds can arise from the interaction of SM particles with the detector materials, QCD hadron and meson events, tau decays, and fake-track coincidental background. Most backgrounds can be reduced to negligible levels by applying an additional invariant mass cut on the displaced jets, where in this paper, the invariant mass $m_{jj} (m_j^{\text{fat}})$ is required to be around the W boson mass, exactly in the range [50, 100] GeV [75, 100]. The remaining potential background arises from fake-track coincidental events, where the tracks of muons and jets from SM sources are accidentally mis-reconstructed around the connections of the hits in the tracker system [101]. In Ref. [101], the fake-track background of pure jets is investigated, which shows that this possible background can be eliminated by applying dedicated

DV fitting variables cuts, such as r_{DV} (transverse distance between the DV and the origin), ΔD_{min} (measure of how well the set of candidate tracks fit in a common vertex), \bar{t} (average of the time coordinate of tracks at the fitted DV), \bar{z} (averaged z -coordinate of tracks at the fitted DV) and standard deviations of the time and z -coordinates of the constituent tracks at the fitted DV. In this analysis, the existence of muon track can simplify the estimation of this background, because the muons from SM sources are typically prompt, with tracks pointing to the primary interacting point of the muon collider. As a result, with the requirement on the well-reconstructed muon and jet tracks and the invariant mass of dijets or fat jet [99], the SM backgrounds can be effectively suppressed to a negligible level. A dedicated analysis of these backgrounds is beyond the scope of this work and will be discussed in more detail in future studies.

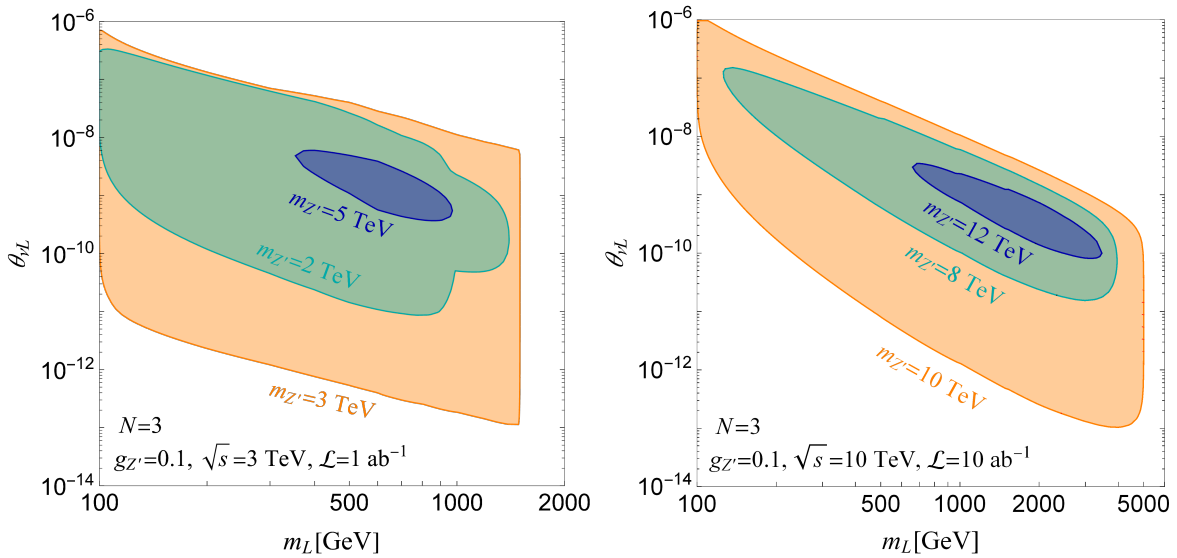


FIG. 6. The expected 95% C.L. sensitivities for the inclusive displaced vertex searches for $\mu^+\mu^- \rightarrow N_L N_L(\gamma)$ with subsequent decay to μW of long-lived sterile neutrino N_L at the muon collider as the function of its mass m_L are shown in the color-shaded regions. The left panel shows the sensitivities for the muon collider with $\mathcal{L} = 1 \text{ ab}^{-1}$ and $\sqrt{s} = 3 \text{ TeV}$, while the right panel shows the sensitivities for the muon collider with $\mathcal{L} = 10 \text{ ab}^{-1}$ and $\sqrt{s} = 10 \text{ TeV}$. The orange-shaded region represents the sensitivity with $m_{Z'} = 3$ (10) TeV, the blue-shaded region represents the sensitivity with $m_{Z'} = 5$ (12) TeV, and the cyan-shaded region represent the sensitivity with $m_{Z'} = 2$ (8) TeV combining $\mu^+\mu^- \rightarrow N_L N_L$ and $\mu^+\mu^- \rightarrow N_L N_L \gamma$ for the left (right) panel.

The sensitivities for probing the long-lived N_L at a 3 TeV muon collider with 95% C.L. are shown in the left panel of Fig. 6 with setting the parameter $g_{Z'} = 0.1$, where the 95% C.L. corresponds to 3 signal events under the assumption of no SM background. We consider 3 benchmark points chosen for $m_{Z'} = 2, 3, 5 \text{ TeV}$, which correspond to cyan, orange, and blue-colored regions, respectively. The most sensitive benchmark point is $m_{Z'} = 3 \text{ TeV}$, because its cross section is

enhanced when $\sqrt{s} = m_{Z'}$, which is more contributed from the N_L pair production. For this $m_{Z'}$ choice, the sensitivity for $\theta_{\nu L}$ can be as low as 10^{-13} . However, the sensitivities decrease rapidly when $m_{Z'}$ moves away from the center of mass energy \sqrt{s} , as shown in the left panel of Fig. 6. When $m_{Z'} < \sqrt{s}$ and $m_{Z'} > 2m_L$, the sensitivity improves due to the higher production cross section of the on-shell Z' , compared to the off-shell case. Specifically, for $m_{Z'} = 2$ TeV and $m_L < 1000$ GeV, the dominant production process is Z' production associated with a photon. The sensitivity is better than that in the case of $m_L > 1000$ GeV, where the dominant process is N_L pair production with a sharply reduced cross section. This results in a noticeable kink in the cyan region around $m_L = 1000$ GeV, as shown in the left panel of Fig. 6. Moreover, at $m_{Z'} = 3$ TeV, the sensitivity exhibits a sharp truncation at $m_L = 1500$ GeV not only due to the rapid decline in the production cross section but also because the process becomes kinematically forbidden when $2m_L > \sqrt{s}$. When Z' mass is even heavier, such as $m_{Z'} = 5$ TeV, the production cross section is much smaller due to phase space suppression, resulting in significantly weaker sensitivity compared to the lighter mass cases. In all these cases, there is a noticeable decrease in sensitivity for light m_L . This reduction of cut efficiency occurs because, when m_L is small, the jets produced from N_L are particularly boosted and collinear, making them difficult to reconstruct independently after processing with Pythia8 and Delphes. Moreover, for lighter m_L , the issue is more severe because, as N_L becomes highly boosted, reconstructing the muon becomes challenging due to the difficulty in isolating muons from jets. This effect is particularly evident for $m_{Z'} = 5$ TeV, where the sensitivity contour is closed.

The sensitivities for probing the long-lived N_L at a 10 TeV muon collider with 95% C.L. are plotted in the right panel of Fig. 6, where we also fixed $g_{Z'} = 0.1$. The benchmark parameter settings chosen are $m_{Z'} = 8, 10,$ and 12 TeV for the cyan, orange, and blue regions in the figure, respectively. The best sensitivity at the muon collider for $\theta_{\nu L}$ can be as good as 10^{-13} for $m_{Z'} = 10$ TeV, where the mass of Z' is equal to \sqrt{s} . Away from the resonance mass, the sensitivities decrease significantly due to the reduction in the signal production cross-section. And their shapes are similar to the $\sqrt{s} = 3$ TeV case. On the other hand, the sensitivity on $\theta_{\nu L}$ at 10 TeV is much weaker relative to the 3 TeV muon collider. For example, for $m_L = 200$ GeV and $m_{Z'} = 3$ (10) TeV, the coupling $\theta_{\nu L}$ in the interval $[3 \times 10^{-12}, 10^{-7}]$ ($[2 \times 10^{-10}, 3 \times 10^{-7}]$) can be probed by the collider with $\sqrt{s} = 3$ (10) TeV and $\mathcal{L} = 1$ (10) ab^{-1} , where the probing interval of $\sqrt{s} = 10$ TeV is somewhat smaller than that of $\sqrt{s} = 3$ TeV, as the production cross section varies inversely with the center-of-mass energy \sqrt{s} . By the way, it is also possible to probe the long-lived sterile

neutrino N_L via the time-delayed method due to its slow-moving signatures, if the detector can record the timing information just like the future CMS [102, 103] and ATLAS [104] at HL-LHC. In this scenario, the ISR photon with a special transverse momentum cut can also stamp the time of N_L generating. But, conservatively, only the traditional displaced vertex method is applied, and we leave the time-delayed approach in our future work.

VI. CONCLUSIONS

In this work, we introduce an UV complete model with a Dirac sterile neutrino charged under the $U(1)_{L_\mu-L_\tau}$ gauge symmetry. After symmetry breaking, this Dirac sterile neutrino splits into two Majorana sterile neutrinos: one heavy sterile neutrino, N_R , which generates the active neutrino mass via a mechanism akin to the type-I seesaw mechanism, and the other naturally long-lived sterile neutrino, N_L . The active neutrino mass, induced by mixing with the sterile neutrino N_R^c , is governed by the parameters $\theta_{\nu R}$ and m_R . The mixing between the left-handed sterile neutrino N_L and the active neutrino ν_L occurs through a two-step process: $N_L \rightarrow N_R^c \rightarrow \nu_L$. As a result, the decay width of N_L is doubly suppressed by the smallness of the active neutrino mass and the small Dirac mass of sterile neutrinos, leading N_L to be long-lived in a collider environment.

We explore the long-lived signatures of N_L at future muon colliders, focusing on the inclusive pair production of N_L via Z' exchange in the s-channel, with and without initial photon radiation. Given the decay branching ratio of N_L , we concentrate on its subsequent decay into a muon and a W boson. Using the displaced vertex method to detect long-lived N_L decays, we find that at a 3 TeV muon collider with an integrated luminosity of 1 ab^{-1} , there is significant sensitivity to sterile neutrino masses in the range $m_L \in [100, 1500] \text{ GeV}$, with mixing angles $10^{-13} < \theta_{\nu L} < 6 \times 10^{-7}$. At a 10 TeV muon collider with an integrated luminosity of 10 ab^{-1} , the sensitivity extends to sterile neutrino masses in the range $m_L \in [100, 5000] \text{ GeV}$, with mixing angles approximately in the range $10^{-13} < \theta_{\nu L} < 10^{-6}$. These long-lived signatures probe new regions of parameter space for the sterile neutrino and complement other constraints from neutrino trident production experiments and muon $g - 2$ measurements.

VII. ACKNOWLEDGMENTS

We thank APCTP, Pohang, Korea, for their hospitality during the focus program [APCTP-2025-F01], from which this work greatly benefited. The work of J. L. is supported by Natural Science Foundation of China under Grants No. 12475103, No. 12235001, and No. 12075005. The work of X. P. W. is supported by the National Science Foundation of China under Grants No. 12375095, and the Fundamental Research Funds for the Central Universities.

-
- [1] R. Davis, Jr., D. S. Harmer, and K. C. Hoffman, *Search for neutrinos from the sun*, Phys. Rev. Lett. **20** (1968) 1205–1209.
 - [2] **KamLAND** Collaboration, K. Eguchi et al., *First results from KamLAND: Evidence for reactor anti-neutrino disappearance*, Phys. Rev. Lett. **90** (2003) 021802, [[hep-ex/0212021](#)].
 - [3] **Daya Bay** Collaboration, F. P. An et al., *Observation of electron-antineutrino disappearance at Daya Bay*, Phys. Rev. Lett. **108** (2012) 171803, [[arXiv:1203.1669](#)].
 - [4] **Double Chooz** Collaboration, Y. Abe et al., *Improved measurements of the neutrino mixing angle θ_{13} with the Double Chooz detector*, JHEP **10** (2014) 086, [[arXiv:1406.7763](#)]. [Erratum: JHEP 02, 074 (2015)].
 - [5] P. Minkowski, *$\mu \rightarrow e\gamma$ at a Rate of One Out of 10^9 Muon Decays?*, Phys. Lett. B **67** (1977) 421–428.
 - [6] T. Yanagida, *Horizontal gauge symmetry and masses of neutrinos*, Conf. Proc. C **7902131** (1979) 95–99.
 - [7] R. N. Mohapatra and G. Senjanovic, *Neutrino Mass and Spontaneous Parity Nonconservation*, Phys. Rev. Lett. **44** (1980) 912.
 - [8] M. Gell-Mann, P. Ramond, and R. Slansky, *Complex Spinors and Unified Theories*, Conf. Proc. C **790927** (1979) 315–321, [[arXiv:1306.4669](#)].
 - [9] J. Kopp, P. A. N. Machado, M. Maltoni, and T. Schwetz, *Sterile Neutrino Oscillations: The Global Picture*, JHEP **05** (2013) 050, [[arXiv:1303.3011](#)].
 - [10] C. Giunti, *Light Sterile Neutrinos: Status and Perspectives*, Nucl. Phys. B **908** (2016) 336–353, [[arXiv:1512.04758](#)].
 - [11] W.-Y. Keung and G. Senjanovic, *Majorana Neutrinos and the Production of the Right-handed Charged Gauge Boson*, Phys. Rev. Lett. **50** (1983) 1427.

- [12] T. Han and B. Zhang, *Signatures for Majorana neutrinos at hadron colliders*, Phys. Rev. Lett. **97** (2006) 171804, [[hep-ph/0604064](#)].
- [13] F. del Aguila, J. A. Aguilar-Saavedra, and R. Pittau, *Heavy neutrino signals at large hadron colliders*, JHEP **10** (2007) 047, [[hep-ph/0703261](#)].
- [14] Y. Cai, T. Han, T. Li, and R. Ruiz, *Lepton Number Violation: Seesaw Models and Their Collider Tests*, Front. in Phys. **6** (2018) 40, [[arXiv:1711.02180](#)].
- [15] E. Accomando, L. Delle Rose, S. Moretti, E. Olaiya, and C. H. Shepherd-Themistocleous, *Extra Higgs boson and Z' as portals to signatures of heavy neutrinos at the LHC*, JHEP **02** (2018) 109, [[arXiv:1708.03650](#)].
- [16] G. Cvetič, A. Das, and J. Zamora-Saá, *Probing heavy neutrino oscillations in rare W boson decays*, J. Phys. G **46** (2019) 075002, [[arXiv:1805.00070](#)].
- [17] A. Das, N. Okada, S. Okada, and D. Raut, *Probing the seesaw mechanism at the 250 gev ilc*, Physics Letters B **797** (Oct., 2019) 134849.
- [18] J. Schechter and J. W. F. Valle, *Neutrino Masses in $SU(2) \times U(1)$ Theories*, Phys. Rev. D **22** (1980) 2227.
- [19] J. Schechter and J. W. F. Valle, *Neutrino Decay and Spontaneous Violation of Lepton Number*, Phys. Rev. D **25** (1982) 774.
- [20] E. K. Akhmedov, M. Lindner, E. Schnapka, and J. W. F. Valle, *Left-right symmetry breaking in NJL approach*, Phys. Lett. B **368** (1996) 270–280, [[hep-ph/9507275](#)].
- [21] E. K. Akhmedov, M. Lindner, E. Schnapka, and J. W. F. Valle, *Dynamical left-right symmetry breaking*, Phys. Rev. D **53** (1996) 2752–2780, [[hep-ph/9509255](#)].
- [22] S. M. Barr, *A Different seesaw formula for neutrino masses*, Phys. Rev. Lett. **92** (2004) 101601, [[hep-ph/0309152](#)].
- [23] D. Wyler and L. Wolfenstein, *Massless Neutrinos in Left-Right Symmetric Models*, Nucl. Phys. B **218** (1983) 205–214.
- [24] R. N. Mohapatra and J. W. F. Valle, *Neutrino Mass and Baryon Number Nonconservation in Superstring Models*, Phys. Rev. D **34** (1986) 1642.
- [25] R. N. Mohapatra, *Mechanism for Understanding Small Neutrino Mass in Superstring Theories*, Phys. Rev. Lett. **56** (1986) 561–563.
- [26] A. Das and N. Okada, *Inverse seesaw neutrino signatures at the LHC and ILC*, Phys. Rev. D **88** (2013) 113001, [[arXiv:1207.3734](#)].

- [27] **Planck** Collaboration, N. Aghanim et al., *Planck 2018 results. VI. Cosmological parameters*, Astron. Astrophys. **641** (2020) A6, [[arXiv:1807.06209](#)]. [Erratum: Astron. Astrophys. 652, C4 (2021)].
- [28] E. Di Valentino, S. Gariazzo, and O. Mena, *Most constraining cosmological neutrino mass bounds*, Phys. Rev. D **104** (2021), no. 8 083504, [[arXiv:2106.15267](#)].
- [29] M. Drewes, A. Giammanco, J. Hajer, and M. Lucente, *New long-lived particle searches in heavy-ion collisions at the LHC*, Phys. Rev. D **101** (2020), no. 5 055002, [[arXiv:1905.09828](#)].
- [30] C. O. Dib, C. S. Kim, and S. Tapia Araya, *Search for light sterile neutrinos from W^\pm decays at the LHC*, Phys. Rev. D **101** (2020), no. 3 035022, [[arXiv:1903.04905](#)].
- [31] M. Drewes and J. Hajer, *Heavy Neutrinos in displaced vertex searches at the LHC and HL-LHC*, JHEP **02** (2020) 070, [[arXiv:1903.06100](#)].
- [32] K. Bondarenko, A. Boyarsky, M. Ovchinnikov, O. Ruchayskiy, and L. Shchutska, *Probing new physics with displaced vertices: muon tracker at CMS*, Phys. Rev. D **100** (2019), no. 7 075015, [[arXiv:1903.11918](#)].
- [33] R. Beltrán, G. Cottin, J. C. Helo, M. Hirsch, A. Titov, and Z. S. Wang, *Long-lived heavy neutral leptons at the LHC: four-fermion single- N_R operators*, JHEP **01** (2022) 044, [[arXiv:2110.15096](#)].
- [34] G. Cottin, J. C. Helo, M. Hirsch, A. Titov, and Z. S. Wang, *Heavy neutral leptons in effective field theory and the high-luminosity LHC*, JHEP **09** (2021) 039, [[arXiv:2105.13851](#)].
- [35] **CMS** Collaboration, A. Hayrapetyan et al., *Search for long-lived heavy neutral leptons in proton-proton collision events with a lepton-jet pair associated with a secondary vertex at $\sqrt{s} = 13$ TeV*, [[arXiv:2407.10717](#)].
- [36] **CMS** Collaboration, A. Hayrapetyan et al., *Search for long-lived heavy neutral leptons decaying in the CMS muon detectors in proton-proton collisions at $s=13$ TeV*, Phys. Rev. D **110** (2024) 012004, [[arXiv:2402.18658](#)].
- [37] J. C. Helo, M. Hirsch, and S. Kovalenko, *Heavy neutrino searches at the LHC with displaced vertices*, Phys. Rev. D **89** (2014) 073005, [[arXiv:1312.2900](#)]. [Erratum: Phys. Rev. D 93, 099902 (2016)].
- [38] S. Antusch, E. Cazzato, and O. Fischer, *Sterile neutrino searches via displaced vertices at LHCb*, Phys. Lett. B **774** (2017) 114–118, [[arXiv:1706.05990](#)].
- [39] J. C. Helo, M. Hirsch, and Z. S. Wang, *Heavy neutral fermions at the high-luminosity LHC*, JHEP **07** (2018) 056, [[arXiv:1803.02212](#)].

- [40] J. Liu, Z. Liu, L.-T. Wang, and X.-P. Wang, *Seeking for sterile neutrinos with displaced leptons at the LHC*, JHEP **07** (2019) 159, [[arXiv:1904.01020](#)].
- [41] CMS Collaboration, A. Tumasyan et al., *Search for long-lived heavy neutral leptons with displaced vertices in proton-proton collisions at $\sqrt{s} = 13$ TeV*, JHEP **07** (2022) 081, [[arXiv:2201.05578](#)].
- [42] A. N. Skrinsky and V. V. Parkhomchuk, *Cooling Methods for Beams of Charged Particles. (In Russian)*, Sov. J. Part. Nucl. **12** (1981) 223–247.
- [43] D. Neuffer, *Principles and Applications of Muon Cooling*, Conf. Proc. C **830811** (1983) 481–484.
- [44] D. Neuffer, *Multi-TeV muon colliders*, AIP Conf. Proc. **156** (1987) 201–208.
- [45] V. D. Barger, M. S. Berger, J. F. Gunion, and T. Han, *s channel Higgs boson production at a muon muon collider*, Phys. Rev. Lett. **75** (1995) 1462–1465, [[hep-ph/9504330](#)].
- [46] V. D. Barger, M. S. Berger, J. F. Gunion, and T. Han, *Higgs Boson physics in the s channel at $\mu^+\mu^-$ colliders*, Phys. Rept. **286** (1997) 1–51, [[hep-ph/9602415](#)].
- [47] C. M. Ankenbrandt et al., *Status of muon collider research and development and future plans*, Phys. Rev. ST Accel. Beams **2** (1999) 081001, [[physics/9901022](#)].
- [48] M. Boscolo, J.-P. Delahaye, and M. Palmer, *The future prospects of muon colliders and neutrino factories*, Rev. Accel. Sci. Tech. **10** (2019), no. 01 189–214, [[arXiv:1808.01858](#)].
- [49] J. P. Delahaye, M. Diemoz, K. Long, B. Mansoulié, N. Pastrone, L. Rivkin, D. Schulte, A. Skrinsky, and A. Wulzer, *Muon Colliders*, [arXiv:1901.06150](#).
- [50] K. Long, D. Lucchesi, M. Palmer, N. Pastrone, D. Schulte, and V. Shiltsev, *Muon colliders to expand frontiers of particle physics*, Nature Phys. **17** (2021), no. 3 289–292, [[arXiv:2007.15684](#)].
- [51] H. Al Ali et al., *The muon Smasher’s guide*, Rept. Prog. Phys. **85** (2022), no. 8 084201, [[arXiv:2103.14043](#)].
- [52] C. Aime et al., *Muon Collider Physics Summary*, [arXiv:2203.07256](#).
- [53] K. M. Black et al., *Muon Collider Forum report*, JINST **19** (2024), no. 02 T02015, [[arXiv:2209.01318](#)].
- [54] T. Bose et al., *Report of the Topical Group on Physics Beyond the Standard Model at Energy Frontier for Snowmass 2021*, [arXiv:2209.13128](#).
- [55] M. Narain et al., *The Future of US Particle Physics - The Snowmass 2021 Energy Frontier Report*, [arXiv:2211.11084](#).
- [56] C. Accettura et al., *Towards a muon collider*, Eur. Phys. J. C **83** (2023), no. 9 864, [[arXiv:2303.08533](#)]. [Erratum: Eur.Phys.J.C 84, 36 (2024)].

- [57] T. Han, D. Liu, I. Low, and X. Wang, *Electroweak couplings of the Higgs boson at a multi-TeV muon collider*, Phys. Rev. D **103** (2021), no. 1 013002, [[arXiv:2008.12204](#)].
- [58] W. Yin and M. Yamaguchi, *Muon $g-2$ at a multi-TeV muon collider*, Phys. Rev. D **106** (2022), no. 3 033007, [[arXiv:2012.03928](#)].
- [59] W. Liu and K.-P. Xie, *Probing electroweak phase transition with multi-TeV muon colliders and gravitational waves*, JHEP **04** (2021) 015, [[arXiv:2101.10469](#)].
- [60] R. T. Co, S. Kumar, and Z. Liu, *Searches for heavy QCD axions via dimuon final states*, JHEP **02** (2023) 111, [[arXiv:2210.02462](#)].
- [61] M. Ruhdorfer, E. Salvioni, and A. Wulzer, *Invisible Higgs boson decay from forward muons at a muon collider*, Phys. Rev. D **107** (2023), no. 9 095038, [[arXiv:2303.14202](#)].
- [62] Z. Liu, K.-F. Lyu, I. Mahbub, and L.-T. Wang, *Top Yukawa coupling determination at high energy muon collider*, Phys. Rev. D **109** (2024), no. 3 035021, [[arXiv:2308.06323](#)].
- [63] P. Li, Z. Liu, and K.-F. Lyu, *Higgs boson width and couplings at high energy muon colliders with forward muon detection*, Phys. Rev. D **109** (2024), no. 7 073009, [[arXiv:2401.08756](#)].
- [64] M. E. Cassidy, Z. Dong, K. Kong, I. M. Lewis, Y. Zhang, and Y.-J. Zheng, *Probing the CP structure of the top quark Yukawa at the future muon collider*, JHEP **05** (2024) 176, [[arXiv:2311.07645](#)].
- [65] W. Liu, K.-P. Xie, and Z. Yi, *Testing leptogenesis at the LHC and future muon colliders: A Z' scenario*, Phys. Rev. D **105** (2022), no. 9 095034, [[arXiv:2109.15087](#)].
- [66] T. Li, H. Qin, C.-Y. Yao, and M. Yuan, *Probing heavy triplet leptons of the type-III seesaw mechanism at future muon colliders*, Phys. Rev. D **106** (2022), no. 3 035021, [[arXiv:2205.04214](#)].
- [67] I. Chakraborty, H. Roy, and T. Srivastava, *Searches for heavy neutrinos at multi-TeV muon collider: a resonant leptogenesis perspective*, Eur. Phys. J. C **83** (2023), no. 4 280, [[arXiv:2206.07037](#)].
- [68] O. Mikulenko and M. Marinichenko, *Measuring lepton number violation in heavy neutral lepton decays at the future muon collider*, JHEP **01** (2024) 032, [[arXiv:2309.16837](#)].
- [69] Z. Wang, X.-H. Yang, and X.-Y. Zhang, *CP violation in lepton-number-conserving processes through heavy Majorana neutrinos at future lepton colliders*, Phys. Lett. B **853** (2024) 138643, [[arXiv:2311.15166](#)].
- [70] K. Mękała, J. Reuter, and A. F. Żarnecki, *Optimal search reach for heavy neutral leptons at a muon collider*, Phys. Lett. B **841** (2023) 137945, [[arXiv:2301.02602](#)].
- [71] T. H. Kwok, L. Li, T. Liu, and A. Rock, *Searching for Heavy Neutral Leptons at A Future Muon Collider*, [[arXiv:2301.05177](#)].

- [72] P. Li, Z. Liu, and K.-F. Lyu, *Heavy neutral leptons at muon colliders*, JHEP **03** (2023) 231, [[arXiv:2301.07117](#)].
- [73] T. Li, C.-Y. Yao, and M. Yuan, *Searching for heavy neutral lepton and lepton number violation through VBS at high-energy muon colliders*, JHEP **09** (2023) 131, [[arXiv:2306.17368](#)].
- [74] D. Barducci and A. Dondarini, *Neutrino dipole portal at a high energy μ -collider*, [arXiv:2404.09609](#).
- [75] R.-Y. He, J.-Q. Huang, J.-Y. Xu, F.-X. Yang, Z.-L. Han, and F.-L. Shao, *Heavy Neutral Leptons in Gauged $U(1)_{L_\mu-L_\tau}$ at Muon Collider*, [arXiv:2401.14687](#).
- [76] X. G. He, G. C. Joshi, H. Lew, and R. R. Volkas, *NEW Z-prime PHENOMENOLOGY*, Phys. Rev. D **43** (1991) 22–24.
- [77] P. Cox, C. Han, and T. T. Yanagida, *LHC Search for Right-handed Neutrinos in Z' Models*, JHEP **01** (2018) 037, [[arXiv:1707.04532](#)].
- [78] K. Asai, K. Hamaguchi, N. Nagata, S.-Y. Tseng, and K. Tsumura, *Minimal Gauged $U(1)_{L_\alpha-L_\beta}$ Models Driven into a Corner*, Phys. Rev. D **99** (2019), no. 5 055029, [[arXiv:1811.07571](#)].
- [79] D. Borah, A. Dasgupta, and D. Mahanta, *TeV scale resonant leptogenesis with $L_\mu-L_\tau$ gauge symmetry in light of the muon $g-2$* , Phys. Rev. D **104** (2021), no. 7 075006, [[arXiv:2106.14410](#)].
- [80] G.-y. Huang, F. S. Queiroz, and W. Rodejohann, *Gauged $L_\mu-L_\tau$ at a muon collider*, Phys. Rev. D **103** (2021), no. 9 095005, [[arXiv:2101.04956](#)].
- [81] A. Das, T. Nomura, and T. Shimomura, *Multi muon/anti-muon signals via productions of gauge and scalar bosons in a $U(1)_{L_\mu-L_\tau}$ model at muonic colliders*, Eur. Phys. J. C **83** (2023), no. 9 786, [[arXiv:2212.11674](#)].
- [82] A. Atre, T. Han, S. Pascoli, and B. Zhang, *The Search for Heavy Majorana Neutrinos*, JHEP **05** (2009) 030, [[arXiv:0901.3589](#)].
- [83] CMS Collaboration, V. Khachatryan et al., *Search for heavy Majorana neutrinos in $\mu^\pm\mu^\pm$ + jets events in proton-proton collisions at $\sqrt{s} = 8$ TeV*, Phys. Lett. B **748** (2015) 144–166, [[arXiv:1501.05566](#)].
- [84] ATLAS Collaboration, G. Aad et al., *Search for heavy Majorana neutrinos with the ATLAS detector in pp collisions at $\sqrt{s} = 8$ TeV*, JHEP **07** (2015) 162, [[arXiv:1506.06020](#)].
- [85] CMS Collaboration, A. M. Sirunyan et al., *Search for heavy neutral leptons in events with three charged leptons in proton-proton collisions at $\sqrt{s} = 13$ TeV*, Phys. Rev. Lett. **120** (2018), no. 22 221801, [[arXiv:1802.02965](#)].

- [86] **CMS** Collaboration, A. M. Sirunyan et al., *Search for heavy Majorana neutrinos in same-sign dilepton channels in proton-proton collisions at $\sqrt{s} = 13$ TeV*, JHEP **01** (2019) 122, [[arXiv:1806.10905](#)].
- [87] W. Altmannshofer, S. Gori, M. Pospelov, and I. Yavin, *Neutrino Trident Production: A Powerful Probe of New Physics with Neutrino Beams*, Phys. Rev. Lett. **113** (2014) 091801, [[arXiv:1406.2332](#)].
- [88] W. Altmannshofer, S. Gori, M. Pospelov, and I. Yavin, *Quark flavor transitions in $L_\mu - L_\tau$ models*, Phys. Rev. D **89** (2014) 095033, [[arXiv:1403.1269](#)].
- [89] **CCFR** Collaboration, S. R. Mishra et al., *Neutrino Tridents and W Z Interference*, Phys. Rev. Lett. **66** (1991) 3117–3120.
- [90] **Muon g-2** Collaboration, D. P. Aguillard et al., *Measurement of the Positive Muon Anomalous Magnetic Moment to 0.20 ppm*, Phys. Rev. Lett. **131** (2023), no. 16 161802, [[arXiv:2308.06230](#)].
- [91] D. Borah, S. Mahapatra, P. K. Paul, and N. Sahu, *Scotogenic $U(1)L_\mu-L_\tau$ origin of $(g-2)_\mu$, W-mass anomaly and 95 GeV excess*, Phys. Rev. D **109** (2024), no. 5 055021, [[arXiv:2310.11953](#)].
- [92] J. P. Leveille, *The Second Order Weak Correction to $(G-2)$ of the Muon in Arbitrary Gauge Models*, Nucl. Phys. B **137** (1978) 63–76.
- [93] J. Alwall, R. Frederix, S. Frixione, V. Hirschi, F. Maltoni, O. Mattelaer, H. S. Shao, T. Stelzer, P. Torrielli, and M. Zaro, *The automated computation of tree-level and next-to-leading order differential cross sections, and their matching to parton shower simulations*, JHEP **07** (2014) 079, [[arXiv:1405.0301](#)].
- [94] **Muon Collider** Collaboration, N. Bartosik et al., *Simulated Detector Performance at the Muon Collider*, [arXiv:2203.07964](#).
- [95] A. Alloul, N. D. Christensen, C. Degrande, C. Duhr, and B. Fuks, *FeynRules 2.0 - A complete toolbox for tree-level phenomenology*, Comput. Phys. Commun. **185** (2014) 2250–2300, [[arXiv:1310.1921](#)].
- [96] T. Sjostrand, S. Mrenna, and P. Z. Skands, *A Brief Introduction to PYTHIA 8.1*, Comput. Phys. Commun. **178** (2008) 852–867, [[arXiv:0710.3820](#)].
- [97] **DELPHES 3** Collaboration, J. de Favereau, C. Delaere, P. Demin, A. Giammanco, V. Lemaître, A. Mertens, and M. Selvaggi, *DELPHES 3, A modular framework for fast simulation of a generic collider experiment*, JHEP **02** (2014) 057, [[arXiv:1307.6346](#)].

- [98] Q.-H. Cao, J. Guo, J. Liu, Y. Luo, and X.-P. Wang, *Long-lived searches of vectorlike lepton and its accompanying scalar at colliders*, Phys. Rev. D **110** (2024), no. 1 015029, [[arXiv:2311.12934](#)].
- [99] J. J. Heinrich, *Reconstruction of boosted W^\pm and Z^0 bosons from fat jets*, Master's thesis, Copenhagen U., 8, 2014.
- [100] Q.-H. Cao, K. Cheng, and Y. Liu, *Distinguishing Dirac from Majorana Heavy Neutrino at Future Lepton Colliders*, Phys. Rev. Lett. **134** (2025), no. 2 021801, [[arXiv:2403.06561](#)].
- [101] J. Liu, Z. Liu, L.-T. Wang, and X.-P. Wang, *Enhancing Sensitivities to Long-lived Particles with High Granularity Calorimeters at the LHC*, JHEP **11** (2020) 066, [[arXiv:2005.10836](#)].
- [102] **CMS Collaboration** Collaboration, *Technical proposal for a MIP timing detector in the CMS experiment Phase 2 upgrade*, tech. rep., CERN, Geneva, Dec, 2017.
- [103] D. Contardo, M. Klute, J. Mans, L. Silvestris, and J. Butler, *Technical Proposal for the Phase-II Upgrade of the CMS Detector*, tech. rep., Geneva, Jun, 2015. Upgrade Project Leader Deputies: Lucia Silvestris (INFN-Bari), Jeremy Mans (University of Minnesota) Additional contacts: Lucia.Silvestris@cern.ch, Jeremy.Mans@cern.ch.
- [104] C. Allaire et al., *Beam test measurements of Low Gain Avalanche Detector single pads and arrays for the ATLAS High Granularity Timing Detector*, JINST **13** (2018), no. 06 P06017, [[arXiv:1804.00622](#)].